Origin of superconductivity in the Weyl semimetal WTe_{2} under pressure

Pengchao Lu, Joon-Seok Kim, Jing Yang, Hao Gao, Juefei Wu, Dexi Shao, Bin Li, Dawei Zhou, Jian Sun, Deji Akinwande, Dingyu Xing, and Jung-Fu Lin

Phys. Rev. B **94**, 224512 — Published 19 December 2016

DOI: 10.1103/PhysRevB.94.224512

Origin of the superconductivity of Weyl semimetal WTe_2 under pressure

Pengchao Lu[1*], Joon-Seok Kim[2*], Jing Yang[5], Hao Gao[1], Juefei Wu[1], Dexi Shao[1], Bin Li[3], DaWei Zhou[1,4], Jian Sun[1]†, Deji Akinwande[2,6], Dingyu Xing[1], Jung-Fu Lin[5,6,7]†

[1] National Laboratory of Solid State Microstructures, School of Physics and Collaborative Innovation Center of Advanced Microstructures, Nanjing University, Nanjing 210093, China.

[2] Microelectronics Research Center, Department of Electrical and Computer Engineering, The University of Texas at Austin, Austin, TX 78758, USA

[3] College of Science, Nanjing University of Posts and Telecommunications, Nanjing 210023, China

[4] College of Physics and Electronic Engineering, Nanyang Normal University, Nanyang 473061, China

[5] Department of Geological Sciences, Jackson School of Geosciences, The University of Texas at Austin, Austin, TX 78712, USA

[6] Texas Materials Institute, The University of Texas at Austin, Austin, TX 78712, USA

[7] Center for High Pressure Science & Technology Advanced Research (HPSTAR), Shanghai 201203, People's Republic of China

*These authors contributed equally to this work. †Correspondence and requests for materials should be addressed to J.S. (e-mail: jiansun@nju.edu.cn) or J.F.L. (e-mail: afu@jsg.utexas.edu)

Abstract

The structure and superconductivity of WTe_2 under pressure are investigated using ab initio calculations combined with high-pressure synchrotron X-ray diffraction and Raman spectroscopy. We find that the emergence of superconductivity in WTe_2 under pressure can be attributed to the phase transition from ambient T_d phase to the monoclinic 1T' structure phase at around 4-5 GPa, which is associated with a sliding of the WTe_2 layers resulting in a critical point in the changes of Te-Te interlayer distance. This phase transition introduces an inversion center and eliminates the topological Weyl fermions in the T_d structure. Electron-phonon coupling calculations predict a similar T_c as reported value, implying that WTe_2 might belong to conventional normal BCS superconductors.

I. INTRODUCTION

2D transition-metal dichalcogenides (TMDs) have recently become one of the most extensively investigated materials due to their unique properties including tunable electronic and transport properties, high mechanical flexibility, and their potential applications in vertical fabricated devices. [1-5] Among the Group VIb element TMDs, tungsten ditelluride (WTe_2) has recently been reported to possess a number of extraordinary physical properties. For instance, a large unsaturated magnetoresistance effect has been observed under a magnetic field of up to 60 Tesla at cryogenic temperatures below 4.5 K [6]. The enhanced magnetoresistance was first described as a result of the symmetric balance between electron and hole pockets on the Fermi surface [7-11], however recent studies have suggested that other mechanisms can play a role in the origin of the magnetoresistance. [12-14] Additionally, WTe_2 was recently proposed as a candidate for a new type of Weyl semimetal (WSM) (Type II) in which the Weyl points exist at the boundary of electron and hole pockets, rather than at the point-like Fermi surface in traditional WSM (Type I) systems. [15-17]

Recently, pressure-induced superconductivity in WTe_2 was observed by two different groups [18,19], but the critical pressure for the emergence of the superconductivity varies from 2.5 GPa to 10.5 GPa in these reports. The superconducting critical temperature (Tc) reaches a maximum of around 6-7 K at certain pressure and decreases with compression to form a dome-like diagram [18,19]. Furthermore, a quantum phase transition is proposed to occur from high-pressure electrical resistance measurements and the pressure-dependent Hall coefficient with a sign changing from the positive to the negative at around 10.5 GPa [19]. However, the relation between the structural parameters of the superconducting phase and the mechanism of the superconductivity in WTe_2 under pressure remains to be elucidated. A clear structural phase transition has not been thoroughly explored along with the emergence of superconductivity [18,19].

WTe_2 crystallizes in the orthorhombic structure with a distorted octahedral coordination (T_d) (space group $Pmn2_1$, No. 31) under ambient conditions [20], which is uniquely different from the typical trigonal prismatic structure in other TMDs, such as the 2H-MoS_2, 2H-WSe_2 (space group $P6_3/mmc$, No. 194) [21] or the monoclinic structure 1T'-$MoTe_2$ (space group $P2_1/m$, No. 11) [20]. Since the crystal structure of WTe_2 is different from other TMDs at ambient conditions, it is reasonable to assume that the crystal structure of WTe_2 at high pressures may play a significant role in the origin of these aforementioned unique physical properties. However, despite its significance, high-pressure phase stability of WTe_2 remains largely unknown and has hindered our understanding of the fundamental physics of the TMDs system in extreme environments.

In this Letter, to give new insights on the aforementioned scientific issues, we explore the structures of WTe_2 under pressure up to 30 GPa, with a combination of ab initio calculations and experiments including high pressure synchrotron powder X-ray diffraction and Raman measurements. We have predicted two high-pressure phases in WTe_2 with $P2_1/m$ and $P6_3/mmc$ symmetry, which resemble the most common 1T' and 2H structure in TMDs, respectively. Moreover, we have identified the 1T' phase in the high pressure XRD and Raman experiments, and resolved its structure. The T_d to 1T' transition pressure is close to the pressure where superconductivity occurs [18,19], implying that the superconducting WTe_2 is actually in the 1T' phase.

II. METHODS

Ab initio calculations. We use ab initio random structure searching (AIRSS) [22,23] method to find low-enthalpy structures of WTe_2, with system sizes up to 8 formula units per simulation cell during the search. Crystal structure optimization calculations are performed by The Vienna Ab initio simulation package (VASP) [24], with Perdew-Burke-Ernzerhof (PBE) [25] generalized gradient approximation (GGA) exchange-correlation density functional and optB86b functional [26,27,28] together with vdW-DF corrections of Langreth and Lundqvist et al [29]. The cutoff parameter for the wave functions is 400 eV, and k-point meshes are generated through Monkhorst-Pack method with a spacing of $0.02\times2\pi$ Å^{-1}. The phonon calculations are performed by supercell approach implemented in the PHONOPY code [30] together with VASP as the atomic force calculator, adopting a 2×2×2 supercell for 1T' and 2H structure. Electronic structure calculations are performed using full-potential linearized augmented plane-wave (FP-LAPW) method implemented in the WIEN2k [31] package. A 2000 k-point mesh for BZ sampling and 7 for the plane wave cut-off parameter $R_{MT}K_{max}$ are used in the calculation, where R is the minimum LAPW sphere radius and K_{max} is the plane-wave vector cutoff. Spin-orbit coupling is taken into consideration in the second-variational calculation [32]. Transition barriers are calculated through the variable cell NEB (VC-NEB) method [33] implemented in the USPEX code [34]. The electron-phonon coupling (EPC) calculations are performed through the Quantum-ESPRESSO program [35], with a 6×8×4 k-point mesh for EPC matrix and a 3×4×2 q-point mesh for Dynamical matrix. The cutoffs are 60 Ry for the wave functions and 600 Ry for the charge density.

High pressure powder X-ray diffraction (XRD) and Raman experiments. A symmetric diamond anvil cell (DAC) with a pair of diamond culet size 400 μm was used for the high pressure Raman experiments. Re gasket, initially ~250 um thick, was pre-indented to ~40 um, and drilled at the very center to form a diameter of 200 μm for the sample chamber. A piece of WTe_2 sample purchased from 2D Semiconductors was cut into ~20 μm disk and was then placed near the center of the sample chamber, along with a couple of ruby spheres used as the pressure indicator. Ar pressure medium was loaded with the sample in the chamber using gas loading system in the Mineral Physics Lab of the University of Texas at Austin. Raman and ruby spectra were collected using Renishaw inVia Raman spectroscopy system equipped with a 532 nm green laser and 3000 line/mm grating. In order to prevent the sample from thermal damaging, laser power was restricted to <5 mW with integration time up to 5 minutes. Obtained spectral data were then analyzed according to background spectra, and peak position and FWHM extracted using Lorentzian fitting. Samples for XRD experiments were purchased from HQ Graphene, and ground using mortar to form randomly oriented powder. Externally heated DAC (EHDAC) with culet size 500 μm was used for high pressure XRD measurements. TZM gasket was pre-indented down to 37 μm thickness, and was drilled with 180 μm hole in the center. Powder WTe_2 were compressed to disks and stack-loaded in the sample chamber, in order to guarantee sufficient thickness and random orientation. Au particle and ruby were also loaded as pressure indicators. Ne gas was used for pressure transmitting medium. XRD experiments were conducted at GSECARS 13IDD beamline of the Advanced Photon Source, Argonne National Laboratory. An incident X-ray beamtime of approximately 0.3344 Å in wavelength and 2-3 μm in beamsize (FWHM) was used for the experiments, while X-ray diffraction patterns of the sample were collected by a MAR CCD detector. High temperature was applied either by external resistive heating or laser heating.

III. RESULTS AND DISCUSSION

The crystallographic structures of T_d, 1T' and 2H phases are shown in Fig. 1 (a), (b). In the T_d phase, the tungsten atoms are sandwiched between two layers of tellurium atoms in which one layer is rotated 180 degrees with respect to the other, forming the W-Te_6 octahedral coordination. These layers in the T_d and 1T' phase exhibit buckled surface structure, whereas the high-pressure 2H structure only contains flat layers. 1T' structure is very similar to T_d such that it can be constructed from T_d phase with shear strain, which introduces an inversion center. Viewing the structure from the out-of-plane direction (Fig. 1 (b)), tungsten and tellurium atoms are packed in a honeycomb crystal lattice for the 2H structure, similar to graphene or h-BN, but it displays a rather complicated atomic arrangement in T_d and 1T' phase.

Theoretical calculations.

The calculated enthalpy-pressure (ΔH-P) and volume-pressure (V-P) curves of WTe_2 are shown in Fig 1. (c), which clearly show two structural phase transitions, from T_d to 1T' at around 5 GPa and from 1T' to 2H phase at about 10 GPa. T_d structure is found to be thermodynamically stable at ambient conditions, in agreement with the experimental observation [20]. However, the relative enthalpy difference between T_d and 1T' phase is very small, less than 0.15 meV per atom, at ambient pressure. Moreover, calculated lattice parameters and unit cell volumes of T_d and 1T' phase are very close to each other. The 2H phase is thermodynamically stable under high pressure, with a lower enthalpy than that of 1T' phase by 59.3 meV per atom at 30 GPa. As 2H structure with flat layers is more compact than the 1T' structure with buckled layers, there is a sudden drop in unit cell volume for the 1T'-2H transition. Compared with other typical TMDs with flat layers, WTe_2 in ambient condition with uneven surface suggests that applied pressure could act to smooth the layers by providing a compressive strain, and therefore tune the electronic properties of the TMD as well as its structure to a higher symmetry. This can be further justified by comparing with WS_2, which has stable 2H phase at ambient condition, although WS_2 does not undergo any structural phase transition up to 60 GPa [36] nor an abrupt metallization at high pressures.

These octahedrally-coordinated W-Te layers are held together by van der Waals interactions such that the dispersion correction is essential for obtaining proper interlayer spacing in theoretical calculations. As shown in the lattice parameters and volumes at 0 GPa listed in Table 1, normal GGA-PBE functional gives quite large errors on these parameters as compared to the experimental values, while the calculations based on optB86b functional together with vdW-DF correction, that were used in this work, gives errors less than 1.0 %. Phonon dispersion calculations confirm that the 1T'- and 2H-WTe_2 structures are dynamically stable at 0 and 15 GPa, respectively (see APPENDIX FIG. A1). Moreover, the phonon spectra at 0 GPa do not exhibit modes with negative frequencies, indicating that they should be recoverable in decompression to ambient pressure if they could be synthesized experimentally. The results for 1T'-WTe_2 also show that two phonon modes near the A, C and E point undergo softening at 5 GPa.

We have also calculated the transition barriers for T_d-1T' and 1T'-2H transitions using VC-NEB method [33]. As shown in Fig. 2, due to the similarity between T_d and 1T' structure, the transition path can be simply considered using an applied shear strain along b axis. As shear strain does not break any W-Te bond, the barrier between T_d and 1T' phase at 5 GPa is quite small, less than 1 meV/atom. For the 1T'-2H transition however, no smooth transition path without breaking bond exists as 1T' and 2H structures belong to different stacking sequences. To minimize the number of broken bonds, we have fabricated a simple transition path based on in-plane glide.

There are four Te atomic layers in 1T' primitive cell, two next-nearest ones of them are made via a glide along *b* axis in opposite directions, these two glides are carried out in different stages to decrease the energy barrier, which results in two barriers and one intermediate low-energy state. The transition barrier between 1T' and 2H phases is estimated to be around 160 meV/atom at pressure of 10 GPa. Such a high barrier seems to be difficult to overcome in high pressure experiments.

Analysis of the calculated band structures and Fermi surfaces as shown in Fig. 3 suggest 1T'-WTe_2 to be a semimetal as a result of the electron and hole pockets along the Γ-Y direction. There are three bands near the Fermi level, two electron-like bands and one hole-like band, composing the Fermi surface. The shape of the Fermi surface is very sensitive to applied pressure, such that an increase in pressure causes an increase in the size of electron and hole pockets. This relationship indicates that 1T'-WTe_2 undergoes a Lifshitz-like, or so-called electronic topological phase transition under pressure. The band structures and the Fermi surface of the 1T' phase are very similar to those in the T_d phase [6], including a perfect balance between electron and hole pockets, which may cause a large unsaturated magnetoresistance effect on the 1T'-WTe_2 system. Lifshitz transitions, which can be seen in Fig. 3, are where the topology of the Fermi surface develops electron and hole pockets, are reported to coincide with the appearance of the superconductivity in iron/transition-metal based superconductor [37,38]. Application of pressure is an efficient method to tune the lattice constants and thereby atomic interactions, which has been reported to produce new topological phases of materials [39]. This naturally draws the question whether pressure could change the topological properties of WTe_2. However, in the T_d phase, spin degeneracy is broken by the spin-orbital coupling due to the absence of an inversion symmetry, while the spin degeneracy will remain in the 1T’ phase which contains an inversion center. Thus, the Weyl fermions in the ambient T_d phase should disappear after the structure phase transition. In previous works [18,19], it was proposed that superconductivity found in WTe_2 emerges from a suppressed large magnetoresistance (LMR) state under high pressure. The critical pressure of superconductivity around 2.5 GPa is close to the T_d-1T’ transition pressure from this work, it is conceivable that superconductivity in WTe_2 emerges from the 1T’ phase, rather than the T_d phase.

In order to get further understanding of the superconductivity mechanism in the system, we have performed ab-initio calculations for the electron-phonon coupling (EPC) of 1T’-WTe_2 using the density functional perturbation theory [40]. The superconducting transition temperature can be estimated by Allen and Dynes modified McMillan formula [41]: $T_c = \frac{\langle\omega\rangle}{1.20} \exp\left(-\frac{1.04(1+\lambda)}{\lambda-\mu^*(1+0.62\lambda)}\right)$, where the parameter λ is a dimensionless measure of the Eliashberg electron-phonon spectral function $\alpha^2F(\omega)$, expressed as $\lambda = 2\int_0^\infty d\omega\, \alpha^2F(\omega)/\omega$. Using a common value of $\mu^* = 0.1$, the T_c in 1T'-WTe_2 at 10 GPa is estimated to be 2~4 K with different broadening factor, which agrees well with the measurements. [18,19] Theoretical phonon dispersions of 1T'-WTe_2 at 10 GPa are shown in Fig. 4(a). It seems that the low frequency phonon modes indeed have significant contributions to the EPC coupling. One TA vibrational mode (B_u mode) near A point is shown in Fig. 4(b), which is mainly contributed to Te-Te interlayer vibrations. Fig. 4(c) shows the calculated interlayer Te-Te distance and W-Te bond length within the layer of 1T’-WTe_2 as a function of pressure up to 10 GPa. The Te-Te distance exhibits an obvious variation under pressure while the intralayer W-Te bond length is almost unchanged. This implies that the effect of compression is mostly on interlayers because of the unique anisotropy of the van der Waals structure. The slope of the variation of the Te-Te distance exhibits two linear regions: a rapid decrease with increasing pressure until around 4 GPa and a slow decrease with further increase in pressure, which suggests an irregular point with compression. This corresponds to the T_d-to-1T' phase transition, where pressure-induced shear strain re-adjusts Te atoms and also introduces an inversion symmetry. Together with the observation of the pressure-induced superconductivity in $ZrTe_5$ [42] and $MoTe_2$ [43], the softening of the interlayer Te-Te vibration modes, resulting from compression of zig-zag TMD layers, can be reasonably correlated with the emergence of the superconductivity in TMDs.

High-pressure experiments

To check our theoretical predictions, we perform high pressure synchrotron X-ray diffraction (XRD) and Raman experiments. Analysis of the high pressure XRD spectra has confirmed the theoretically-predicted T_d-1T' transition. In the simulated XRD patterns in Fig. 5(a), the 1T' phase can be effectively distinguished from T_d phase by splitting of (011) and (113) peaks. Evolution of the experimental patterns as pressure increases in Fig. 5(b) clearly shows such splitting, despite somewhat broad peaks due to the existence of deviatoric stress under high pressures. The diffraction signal of 1T' phase first appears at around 4 GPa, which agrees very well with the theoretical prediction (Fig. 5(b), violet lines). After applying external heating to ~350 K at high pressures, the 1T' diffraction signal is significantly enhanced and becomes dominant at higher pressure/temperature (Fig. 5(b), red lines). A representative experimental XRD spectrum of WTe_2 is compared with theoretical prediction of 1T' and T_d phase, which resembles 1T' phase in overall range of the spectra (Fig. 5(a)). The T_d and 1T' structure can be fitted to the XRD patterns measured at 1.4 and 7.6 GPa, respectively, as shown in Fig. 5(c), (d). Le Bail method was used to fit the experimental XRD data, because WTe_2 is intrinsically layered and therefore can develop textures at high pressures which hinders Rietveld refinement to provide suitable analysis. We note that the 1T’-to-2H phase transition was not observed in the high pressure experiment, even with increased temperature; up to 22.9 GPa and 450 K for externally heated DAC (EHDAC), and 15.4 GPa and >2000 K for laser heated DAC (LHDAC), respectively. This is consistent with our calculations on transition barriers, where the transition barrier from 1T’ to 2H is significantly high. The transition may be a sluggish process due to the high kinetic barriers, and therefore the equilibration time during the experiment was not long enough to fully transform to 2H phase, even if the applied pressure and temperature were sufficiently high. As forming alloyed MoTe2−WTe2 monolayers can decrease critical temperatures of T’-H transition efficiently [44], introducing Mo-doping may scale down the transition pressure of 1T’-2H transition in bulk WTe2. Because the main focus of present study is to relate superconductivity to the structural phase of WTe_2 at relatively low pressures, while the 2H phase is estimated to be semiconducting below 18 GPa (see APPENDIX FIG. A2), thus no additional experiments were designed to apply higher pressure and temperature.

High pressure Raman measurements also suggest the occurrence of a structural phase transition at around 11 GPa. There are thirty-three irreducible representations of the optical phonons in T_d-WTe_2 at the Gamma point for the C_{2v} (mm2) group: $\Gamma_{optic} = 11A_1 + 6A_2 + 5B_1 + 11B_2$, which are all Raman active. Seven of them are observed in laser spectroscopic experiments for the T_d structure under ambient pressure [45,46] including A_1 (78.9 cm^{-1}), A_2 (88.4 cm^{-1}), A_2 (109.9 cm^{-1}), A_1 (114.6 cm^{-1}), A_1 (129.9 cm^{-1}), A_1 (160.6 cm^{-1}), and A_1 (207.7 cm^{-1}) [45]. For the 1T’ structure with the point group C_{2h} (2/m), there are thirty-three optic modes at the Gamma point as well: $\Gamma_{optic} = 12A_g + 5A_u + 6B_g + 10B_u$. Eighteen of them, $12A_g + 6B_g$, are Raman active modes. The evolution of these modes under high pressure is shown in Fig. 6. Six Raman peaks measured in ambient pressure, denoted as P1, P2, P3, P5, P6, and P7, undergo blueshift as pressure increases, where the overall trend shows a good match with calculated results up to 30 GPa. The discontinuity of Raman bands above 11 GPa, such as the vanishing P3 band and the occurrence of the P4 band with a higher frequency, suggests that T_d-1T' transition has occurred (see Fig. 6(a)). As shown in Fig. 6(b), the pressure dependence of the FWHM of the Raman bands P6 and P7 rapidly increased from -0.02 cm^{-1}/GPa to 0.25 cm^{-1}/GPa and from -0.05 cm^{-1}/GPa to 0.19 cm^{-1}/GPa, respectively, at ~11 GPa. When compared to the relatively slow broadening of P1 (-0.1 cm^{-1}/GPa to 0.07 cm^{-1}/GPa) and P2 band which both remain sharp at high pressure (Fig. 6(a)), broadening of P6 and P7 may be attributed to the appearance of the 1T' phase.

IV. CONCLUSION

In summary, the combination of the crystal structural prediction and first-principles calculations in this study allows us to predict that WTe_2 undergoes two structural phase transitions: T_d ($Pmn2_1$) to 1T’ ($P2_1/m$) transition at around 4-5 GPa and 1T’ ($P2_1/m$) to 2H ($P6_3/mmc$) phase at around 10 GPa. High-pressure XRD and Raman measurements confirm the T_d-1T’ transition and give consistent critical transition pressure at around 4-5 GPa. Since the transition pressure is very close to the emergence pressure of the superconductivity and that the irregular points in the Te-Te distance variations and modes softening in the phonon spectra occur across the transition, we thus attribute the pressure-induced superconductivity in WTe_2 to T_d-1T’ structure transition. Based on the analysis of the transition path and energy barriers, we find that the barrier for the T_d-1T’ transition is very low and the one for the 1T'-2H transition is very high. The latter is likely the reason why the 2H phase has not been observed experimentally. These results show that applied pressure not only influences the stacking sequences but also the electronic structures of the layered TMD materials, giving rise to very rich electronic features of WTe_2 at high pressures and low temperatures.

Acknowledgements

We acknowledge the financial support from MOST of China (Grant Nos: 2016YFA0300404, 2015CB921202), the National Natural Science Foundation of China (Grant Nos: 51372112 and 11574133), NSF Jiangsu province (No. BK20150012), the Fundamental Research Funds for the Central Universities and Special Program for Applied Research on Super Computation of the NSFC-Guangdong Joint Fund (the second phase). D.A acknowledges support from DTRA and ARO. JFL acknowledges support from HPSTAR Program. High-pressure XRD experiments were conducted at GSECARS of the Advanced Photon Source. The authors thank V. Prakapenka, J. Gao, J. Zhou, and X. Li for their assistance and advice in the X-ray diffraction experiments and analysis. Part of the calculations were performed on the supercomputer in the High Performance Computing Center of Nanjing University.

References

[1] K. F. Mak, C. Lee, J. Hone, J. Shan, and T.F. Heinz, Phys. Rev. Lett. 105, 136805 (2010).

[2] C. Lee, H. Yan, L. E. Brus, T. F. Heinz, J. Hone, and S. Ryu, ACS Nano 4 (5), pp 2695–2700 (2010).

[3] Avinash P. Nayak, Tribhuwan Pandey, Damien Voiry, Jin Liu, Samuel T. Moran, Ankit Sharma, Cheng Tan, Chang-Hsiao Chen, Lain-Jong Li, Manish Chhowalla, Jung-Fu Lin, Abhishek K. Singh, and Deji Akinwande, Nano Lett. 15 (1), pp 346–353 (2015).

[4] Avinash P. Nayak, Swastibrata Bhattacharyya, Jie Zhu, Jin Liu, Xiang Wu, Tribhuwan Pandey, Changqing Jin, Abhishek K. Singh, Deji Akinwande, and Jung-Fu Lin, Nat. Commun. 5, 3731 (2014).

[5] A. K. Geim and I. V. Grigorieva, Nature 499, 419 (2013).

[6] M. N. Ali, J. Xiong, S. Flynn, J. Tao, Q. D. Gibson, L. M. Schoop, T. Liang, N. Haldolaarachchige, M. Hirschberger, N. P. Ong, and R. J. Cava, Nature 514, 205 (2014).

[7] H. Y. Lv, W. J. Lu, D. F. Shao, Y. Liu, S. G. Tan and Y. P. Sun, Europhys. Lett. 110, 37004 (2015).

[8] Zengwei Zhu, Xiao Lin, Juan Liu, Benoît Fauqué, Qian Tao, Chongli Yang, Youguo Shi, and Kamran Behnia, Phys. Rev. Lett. 114, 176601 (2015).

[9] I. Pletikosić, Mazhar N. Ali, A.□V. Fedorov, R.□J. Cava, and T. Valla, Phys. Rev. Lett. 113, 216601 (2014).

[10] F. Xiang, M. Veldhorst, S. Dou, and X. Wang, Europhys. Lett. 112, 37009 (2015).

[11] P.□L. Cai, J. Hu, L.□P. He, J. Pan, X.□C. Hong, Z. Zhang, J. Zhang, J. Wei, Z.□Q. Mao, and S.□Y. Li, Phys. Rev. Lett. 115, 057202 (2015).

[12] M. M. Parish and P. B. Littlewood, Nature 426, 162 (2003).

[13] J. Jiang, F. Tang, X.□C. Pan, H.□M. Liu, X.□H. Niu, Y.□X. Wang, D.□F. Xu, H.□F. Yang, B.□P. Xie, F.□Q. Song, P. Dudin, T.□K. Kim, M. Hoesch, P. Kumar Das, I. Vobornik, X.□G. Wan, and D.□L. Feng, Phys. Rev. Lett. 115, 166601 (2015).

[14] Y. Wang, K. Wang, J. Reutt-Robey, J. Paglione, and M. S. Fuhrer, Phys. Rev. B 93, 121108(R) (2016).

[15] Alexey A. Soluyanov, Dominik Gresch, Zhijun Wang, QuanSheng Wu, Matthias Troyer, Xi Dai, and B. Andrei Bernevig, Nature 527, 495-498 (2015).

[16] F. Y. Bruno, A. Tamai, Q. S. Wu, I. Cucchi, C. Barreteau, A. de la Torre, S. McKeown Walker, S. Riccò, Z. Wang, T. K. Kim, M. Hoesch, M. Shi, N. C. Plumb, E. Giannini, A. A. Soluyanov, and F. Baumberger, Phys. Rev. B 94, 121112(R).

[17] Chenlu Wang, Yan Zhang, Jianwei Huang, Simin Nie, Guodong Liu, Aiji Liang, Yuxiao Zhang, Bing Shen, Jing Liu, Cheng Hu, Ying Ding, Defa Liu, Yong Hu, Shaolong He, Lin Zhao, Li Yu, Jin Hu, Jiang Wei, Zhiqiang Mao, Youguo Shi, Xiaowen Jia, Fengfeng Zhang, Shenjin Zhang, Feng Yang, Zhimin Wang, Qinjun Peng, Hongming Weng, Xi Dai, Zhong Fang, Zuyan Xu, Chuangtian Chen, and X. J. Zhou, arXiv:1604.04218 (2016).

[18] Xing-Chen Pan, Xuliang Chen, Huimei Liu, Yanqing Feng, Zhongxia Wei, Yonghui Zhou, Zhenhua Chi, Li Pi, Fei Yen, Fengqi Song, Xiangang Wan, Zhaorong Yang, Baigeng Wang, Guanghou Wang, and Yuheng Zhang, Nat. Commun. 6, 7805 (2015).

[19] Defen Kang, Yazhou Zhou, Wei Yi, Chongli Yang, Jing Guo, Youguo Shi, Shan Zhang, Zhe

Wang, Chao Zhang, Sheng Jiang, Aiguo Li, Ke Yang, Qi Wu, Guangming Zhang, Liling Sun, and Zhongxian Zhao, Nat. Commun. 6, 7804 (2015).

[20] B. E. Brown, Acta Cryst. 20, 268-274 (1966).

[21] Manish Chhowalla, Hyeon Suk Shin, Goki Eda, Lain-Jong Li, Kian Ping Loh, and Hua Zhang, Nature Chemistry 5, 263–275 (2013).

[22] C. J. Pickard and R. J. Needs, Phys. Rev. Lett. 97, 045504 (2006).

[23] C. J. Pickard and R. J. Needs, J. Phys. Condens. Mat. 23, 053201 (2011).

[24] G. Kresse and J. Furthmüller, Comput. Mater. Sci. 6, 15-50 (1996).

[25] J. P. Perdew, K. Burke, and M. Ernzerhof, Phys. Rev. Lett.77, 3865-3868 (1996).

[26] G. Román-Pérez and J. M. Soler, Phys. Rev. Lett. 103, 096102 (2009).

[27] J. Klimeš, D. R. Bowler, and A. Michaelides, Phys. Rev. B 83, 195131 (2011).

[28] T. Thonhauser, Valentino R. Cooper, Shen Li, Aaron Puzder, Per Hyldgaard, and David C. Langreth, Phys. Rev. B 76, 125112 (2007).

[29] M. Dion, H. Rydberg, E. Schröder, D. C. Langreth, and B. I. Lundqvist, Phys. Rev. Lett. 92, 246401 (2004).

[30] A. Togo, F. Oba, and I. Tanaka, Phys. Rev. B 78, 134106 (2008).

[31] P. Blaha, K. Schwarz, G. Madsen, D. Kvasicka, and J. Luitz, ISBN 3-9501031-1-2 (2002).

[32] J. Kuneš , P. Novák, R. Schmid, P. Blaha, and K. Schwarz, Phys. Rev. B 64, 153102 (2001).

[33] G.R. Qian, X. Dong, X.-F. Zhou, Y. Tian, A.R. Oganov, and H.-T. Wang, Comput. Phys. Commun. 184(9):2111–2118 (2013).

[34] A. R. Oganov and C. W. Glass, J. Chem. Phys. 124, 244704 (2006).

[35] P. Giannozzi, S. Baroni, N. Bonini, M. Calandra, R. Car, C. Cavazzoni, D. Ceresoli, G.L. Chiarotti, M. Cococcioni, I. Dabo, A. Dal Corso, S. de Gironcoli, S. Fabris, G. Fratesi, R. Gebauer, U. Gerstmann, C. Gougoussis, A. Kokalj, M. Lazzeri, L. Martin-Samos, N. Marzari, F. Mauri, R. Mazzarello, S. Paolini, A. Pasquarello, L. Paulatto, C. Sbraccia, S. Scandolo, G. Sclauzero, A. P. Seitsonen, A. Smogunov, P. Umari, and R. M. Wentzcovitch, J. Phys. Condens. Mat. 21, 395502 (2009).

[36] Avinash P. Nayak, Zhen Yuan, Boxiao Cao, Jin Liu, Junjie Wu, Samuel T. Moran, Tianshu Li, Deji Akinwande, Changqing Jin, and Jung-Fu Lin, ACS Nano, 9 (9), pp 9117–9123 (2015).

[37] Chang Liu, Takeshi Kondo, Rafael M. Fernandes, Ari D. Palczewski, Eun Deok Mun, Ni Ni, Alexander N. Thaler, Aaron Bostwick, Eli Rotenberg, Jörg Schmalian, Sergey L. Bud'ko, Paul C. Canfield, and Adam Kaminski, Nat. Phys. 6, 419–423 (2010).

[38] Yun Wu, Na Hyun Jo, Masayuki Ochi, Lunan Huang, Daixiang Mou, Sergey L. Bud'ko, P.□C. Canfield, Nandini Trivedi, Ryotaro Arita, and Adam Kaminski, Phys. Rev. Lett. 115, 166602 (2015).

[39] Y. Zhou, P. Lu, Y. Du, X. Zhu, R. Zhang, D. Shao, X. Chen, X. Wang, M. Tian, J. Sun, X. Wan, Z. Yang, Y. Zhang, D. Xing, arXiv:1509.07361 (2015).

[40] S. Baroni, S. de Gironcoli, A. D. Corso, and P. Giannozzi, Rev. Mod. Phys. 73, 515 (2001).

[41] P. B. Allen and R. C. Dynes, Phys. Rev. B 12, 905 (1975).

[42] Yonghui Zhou, Juefei Wu, Wei Ning, Nana Li, Yongping Du, Xuliang Chen, Ranran Zhang, Zhenhua Chi, Xuefei Wang, Xiangde Zhu, Pengchao Lu, Cheng Ji, Xiangang Wan, Zhaorong Yang, Jian Sun, Wenge Yang, Mingliang Tian, Yuheng Zhang, and Ho-kwang Mao, Proc. Nat. Acad. Sci. USA, 113 (11) 2904-2909 (2016).

[43] Yanpeng Qi, Pavel G. Naumov, Mazhar N. Ali, Catherine R. Rajamathi, Walter Schnelle,

Oleg Barkalov, Michael Hanfland, Shu-Chun Wu, Chandra Shekhar, Yan Sun, Vicky Süß, Marcus Schmidt, Ulrich Schwarz, Eckhard Pippel, Peter Werner, Reinald Hillebrand, Tobias Förster, Erik Kampert, Stuart Parkin, R. J. Cava, Claudia Felser, Binghai Yan, and Sergey A. Medvedev, Nat. Commun. 7, 11038 (2016).

[44] K.-A. N. Duerloo and E. J. Reed, ACS Nano, 10 (1), pp 289–297 (2016).

[45] W.-D. Kong, S.-F. Wu, P. Richard, C.-S. Lian, J.-T. Wang, C.-L. Yang, Y.-G. Shi, and H. Ding, Appl. Phys. Lett. 106, 081906 (2015).

[46] Chia-Hui Lee, Eduardo Cruz-Silva, Lazaro Calderin, Minh An T. Nguyen, Matthew J. Hollander, Brian Bersch, Thomas E. Mallouk, and Joshua A. Robinson, Sci. Rep. 5, 10013 (2015).

Figures

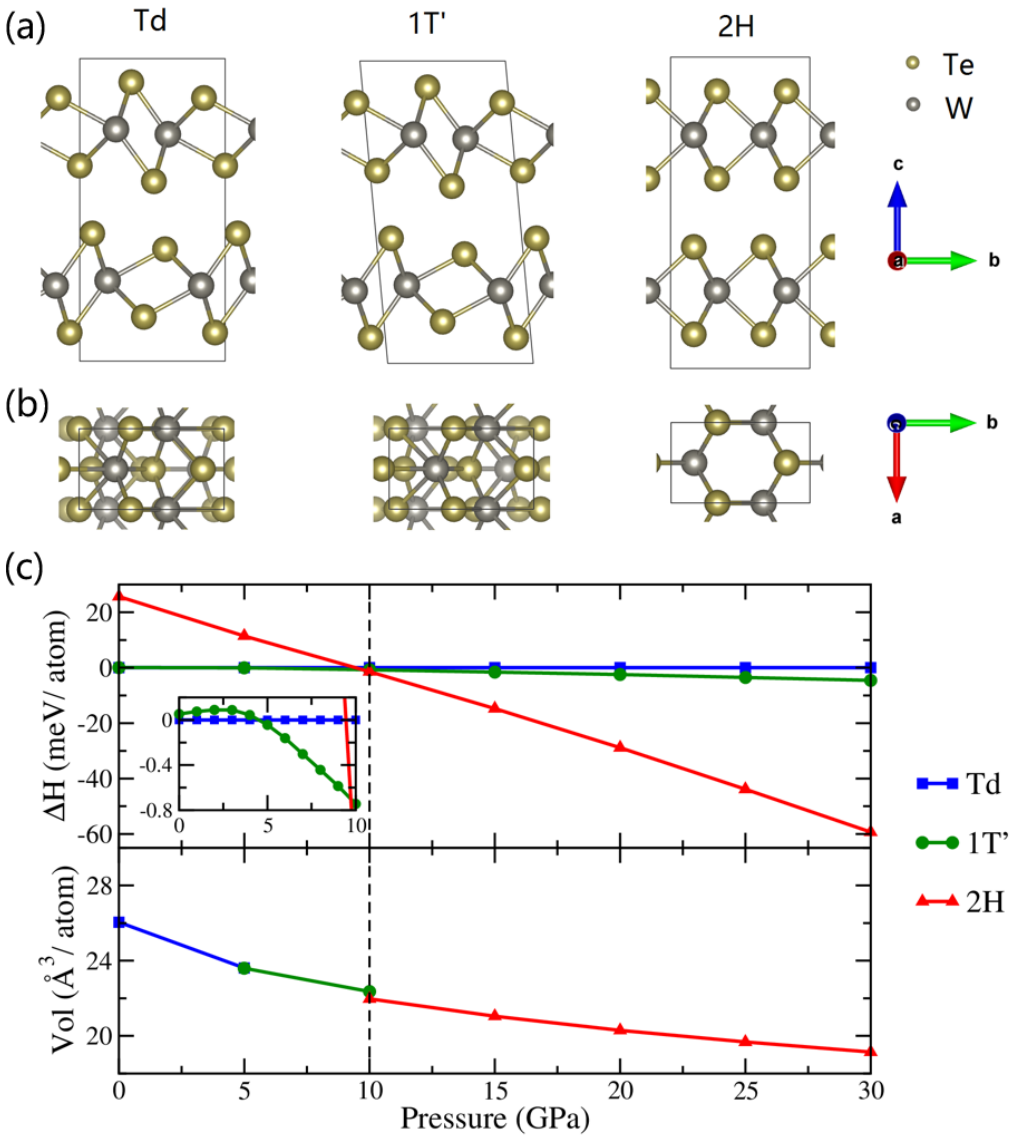

FIG. 1. (a) and (b) Schematic representations of Td, 1T' and 2H crystal structures of WTe_2 along *a* axis and *c* axis, respectively. To compare 2H with Td and 1T', the hexagonal 2H lattice is converted to orthorhombic lattice by building a $1 \times \sqrt{3}$ supercell in the *xy* plane. (c) Relative enthalpy difference between 2H and Td phases as a function of pressure (top panel) and their pressure-volume curves (bottom panel). Theoretical calculations indicate two structural phase transitions, from Td to 1T' at around 5 GPa and from 1T' to 2H phase at about 10 GPa, respectively.

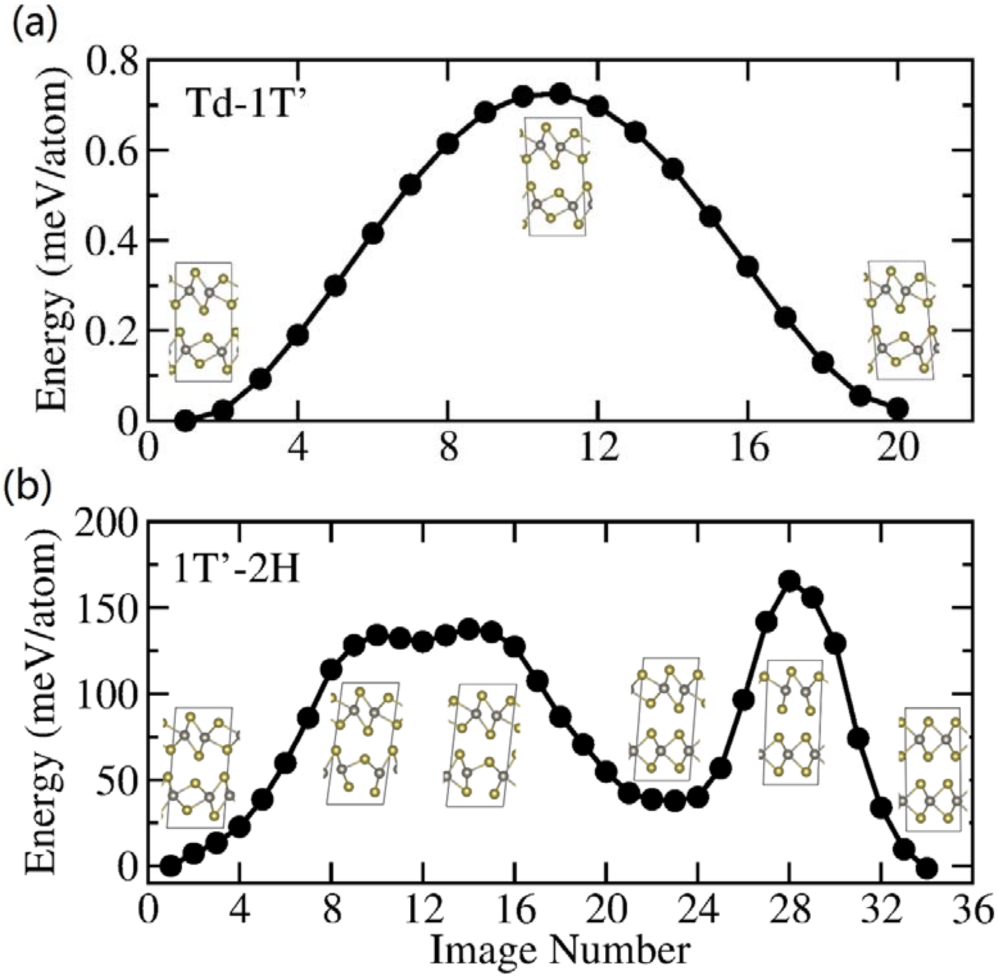

FIG. 2. Enthalpy versus pathway for (a) Td-1T' transition at 5GPa and (b) 1T'-2H transition at 10GPa. The Td-1T’ transition path is considered as shear strain along b axis, while the 1T’-2H transition path is considered as Te atomic layers gliding along b axis, with four bonds broken and rebuilt per cell.

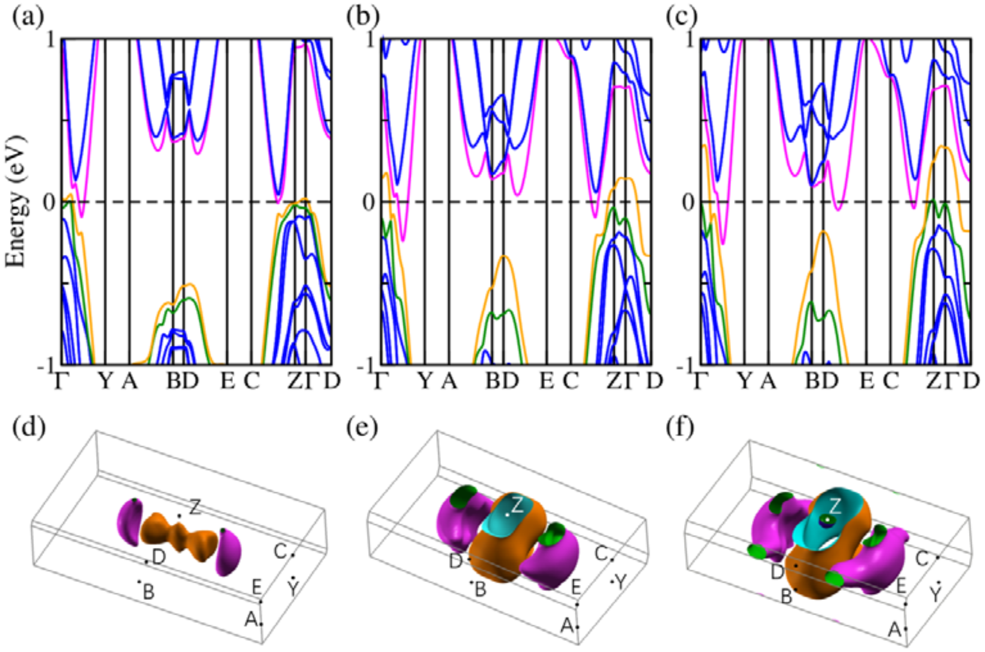

FIG. 3. Calculated band structures and Fermi Surfaces of 1T'-WTe$_2$ with spin-orbital coupling (SOC) at 0 GPa (a),(d), 5 GPa (b),(e), and 10 GPa (c),(f). Three bands near Fermi level, two electron-like bands and one hole-like band, are shown in green, orange and magenta respectively, while other bands are in blue. Due to the coexistence of time-reversal symmetry (TRS) and inversion symmetry, the SOC will not break spin degeneracy in 1T'-WTe$_2$.

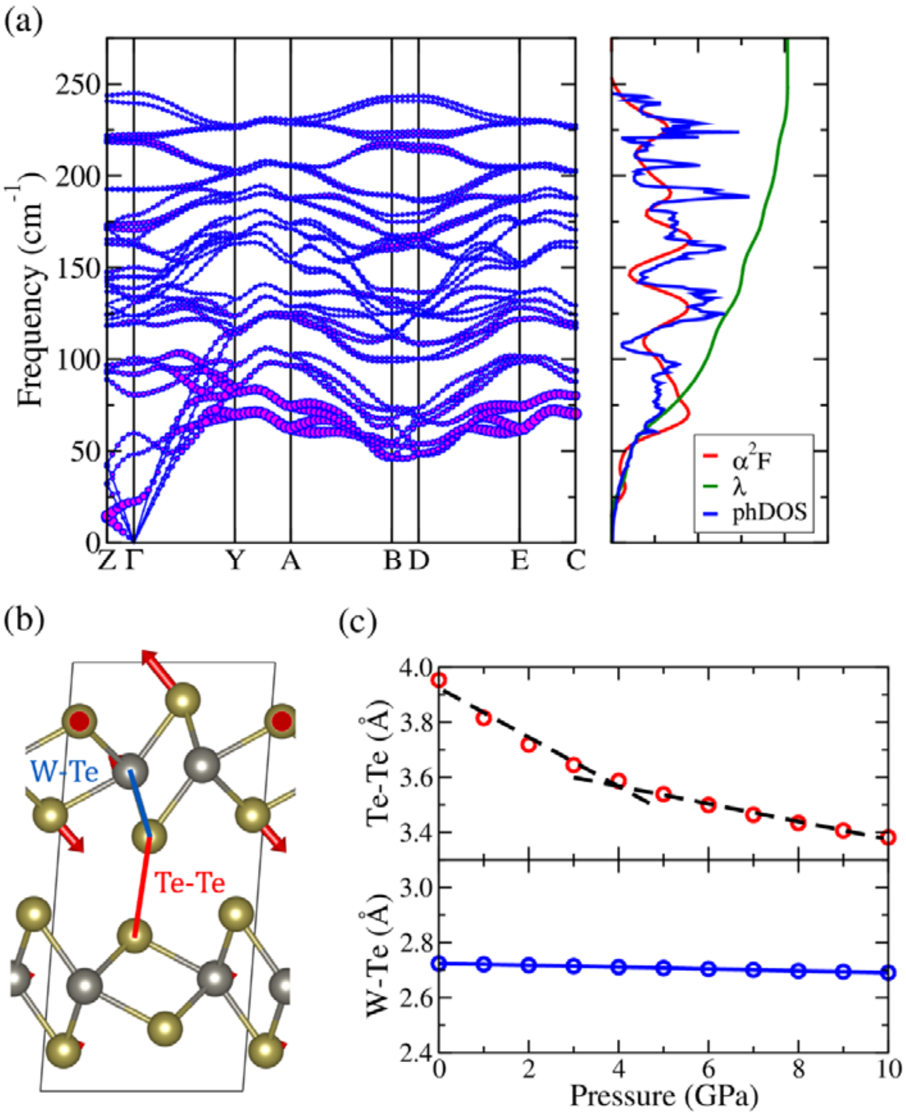

FIG. 4. (a) Theoretical phonon dispersions of 1T'-WTe$_2$ at 10 GPa. The size of the dots represents density of electron-phonon spectral function . Phonon DOS and the electron-phonon integral λ(ω) are also shown on the right panel. (b) Schematic representations of 1T'-WTe$_2$ crystal structures along *a* axis. Red arrows represent one TA vibrational mode (B$_u$ symmetry) near A point. (c) Theoretical Te-Te bond length (top panel) and W-Te bond length (bottom panel) of 1T'-WTe$_2$ as a function of pressure. The Te-Te bond length shows a rapid decrease with increasing pressure until around 4 GPa and a slow decrease with further increase in pressure. The dashed lines fit for two phases, i.e., the normal 1T' phase and the collapsed 1T', in two pressure region.

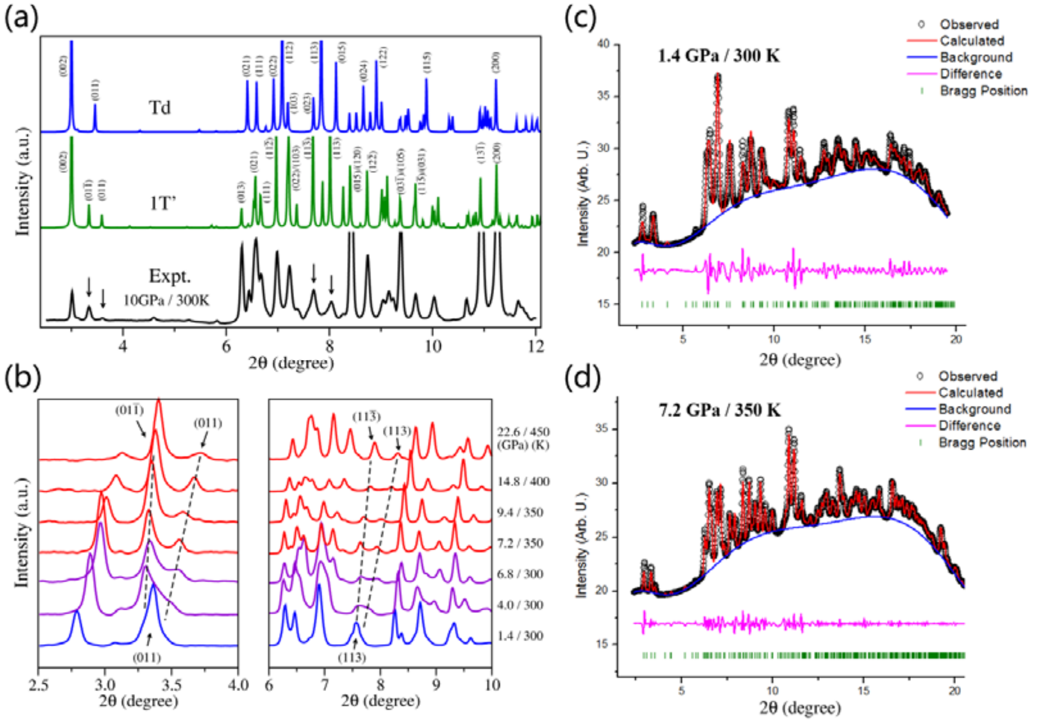

FIG. 5. (a) Simulated XRD patterns of the optimized structures at 10 GPa, compared with experimental values at 10 GPa / 300 K. The wavelength is 0.3344 Å. Black arrows in the experimental spectrum indicates the splitted (011) and (113) peaks. (b) Experimental XRD spectra under high pressure. (011) and (113) peaks clearly shows splitting, which is an evidence of phase transition from Td to 1T’ as pressure/temperature increases. High pressure X-ray powder diffraction spectra for (c) Td phase 1.4 GPa / 300 K, and (d) 1T’ phase 7.2 GPa / 350 K. The two experimental data matched well with calculated Bragg peaks. Le Bail method was used in order to fit the diffraction, where the layered WTe2 has preferred orientations and therefore highly textured structure.

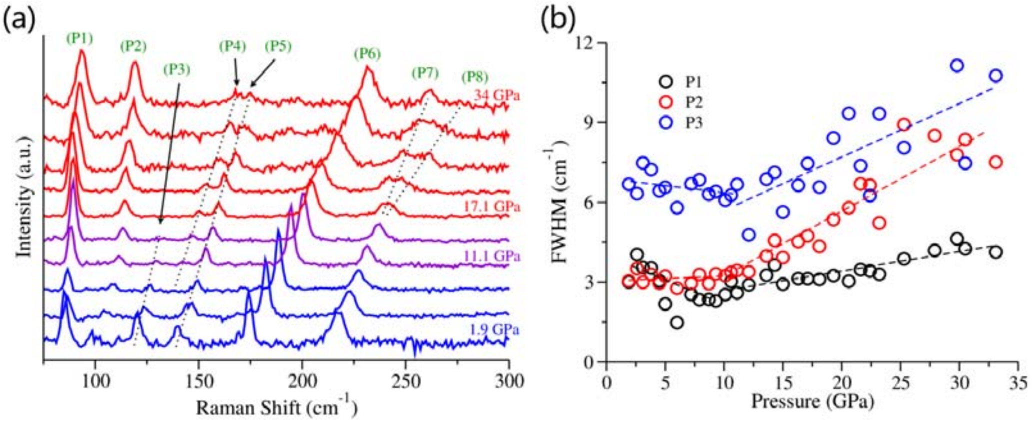

FIG. 6. (a) Experimental Raman spectra of WTe2 under pressure. Dashed lines are guided line of the peaks, showing discontinuity of P3 and P4, and phonon splitting of P8 from P7. (b) FWHM of P1, P6, and P7, indicating dramatic broadening of P6 and P7 at pressure >11 GPa. This implies possible rising of Raman modes in 1T' phase, as predicted from theoretical calculation. Dashed lines are linear fit lines for the range before and after 11 GPa.

Table 1. Calculated lattice parameters and volumes at 0GPa through GGA-PBE functional and optB86b functional with vdW-DF correction, compared with the experimental values from Ref. [20]. Normal GGA-PBE functional gives quite large error as compared to the experimental values, while the calculations based on optB86b-vdW functional, gives error less than 1.0%.

	T_d ($Pmn2_1$)			1T' ($P2_1/m$)		2H ($P6_3/mmc$)	
	PBE	optB86b	Expt.	PBE	optB86b	PBE	optB86b
a	3.500	3.499	3.496	3.500	3.499	3.558	3.533
b	6.328	6.285	6.282	6.327	6.286	3.558	3.533
c	15.803	14.211	14.070	15.612	14.217	15.167	14.110
Volume	350.00	312.52	309.00	345.48	312.42	166.26	152.56

APPENDIX

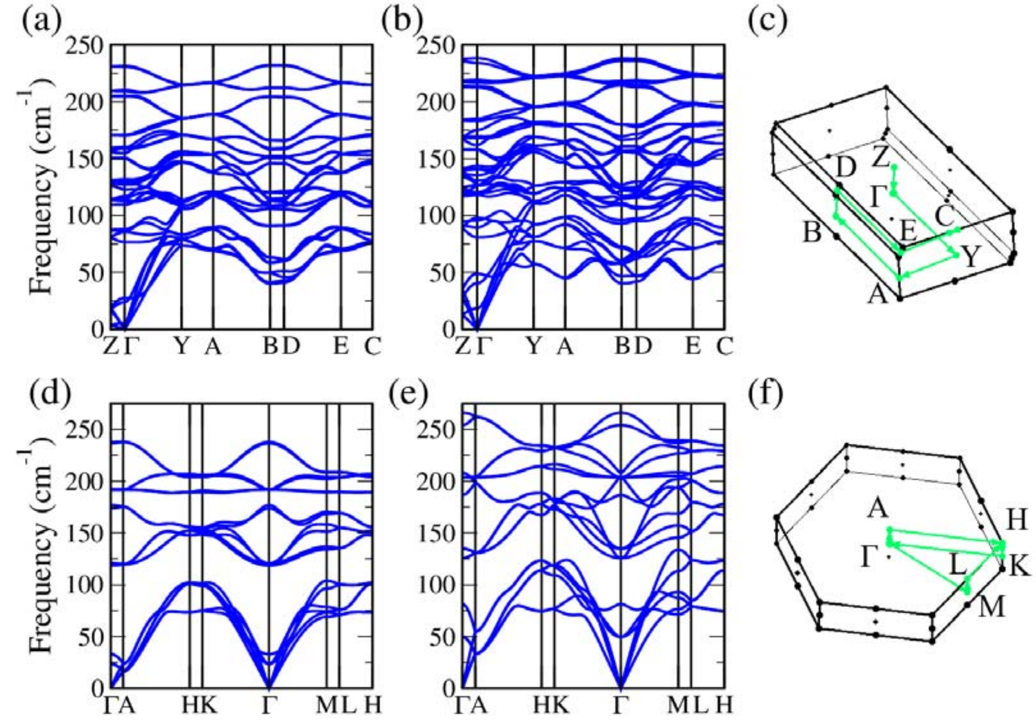

FIG. A1. Phonon dispersion relations of 1T'-WTe$_2$ (a) 0GPa and (b) 5GPa, and 2H-WTe$_2$ at (d) 0GPa and (e) 15GPa, with their first Brillouin zones (c) and (f) respectively. These two structures are confirmed to be dynamically stable as the phonon dispersions exhibit no negative-frequency modes. Moreover, it should be recoverable in decompression to ambient pressure if they could be synthesized experimentally. Two phonon modes near the A, C and E point goes soft in 1T'-WTe2 at 5GPa.

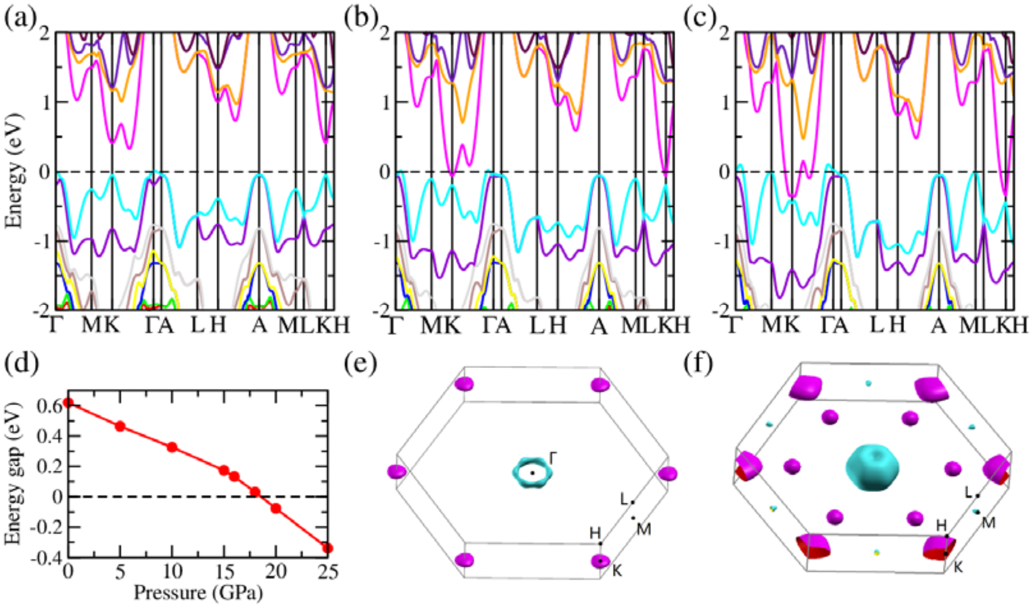

FIG. A2. Calculated band structures of 2H-WTe2 with SOC at 10 GPa (a), 20 GPa (b), 30 GPa (c), energy gap as a function of pressure (d), and Fermi Surface at 20 GPa (e) and 30 GPa (f).